Title
Cell Size Determines the Strength of the Spindle Assembly Checkpoint during Embryonic Development

Journal
Developmental Cell, 36(3)

ISSN
1534-5807

Authors
Galli, Matilde
Morgan, David O

Publication Date
2016-02-01

DOI
10.1016/j.devcel.2016.01.003

Peer reviewed

HHS Public Access

Author manuscript

Dev Cell. Author manuscript; available in PMC 2017 February 08.

Published in final edited form as:

Dev Cell. 2016 February 8; 36(3): 344–352. doi:10.1016/j.devcel.2016.01.003.

Cell size determines the strength of the spindle assembly checkpoint during embryonic development

Matilde Galli[1,2,*] and **David O. Morgan**[1,*]

Matilde Galli: m.galli@hubrecht.eu

[1]Department of Physiology and Department of Biochemistry and Biophysics, University of California, San Francisco, CA 94143, USA

Summary

The spindle assembly checkpoint (SAC) delays mitotic progression when chromosomes are not properly attached to microtubules of the mitotic spindle. Cells vary widely in the extent to which they delay mitotic progression upon SAC activation. To explore the mechanisms that determine checkpoint strength in different cells, we systematically measured the mitotic delay induced by microtubule disruption at different stages of embryogenesis in *Caenorhabditis elegans*. Strikingly, we observed a gradual increase in SAC strength after each round of division. Analysis of mutants that alter cell size or ploidy revealed that SAC strength is determined primarily by cell size and the number of kinetochores. These findings provide clear evidence *in vivo* that the kinetochore-to-cytoplasm ratio determines the strength of the SAC, providing new insights into why cells exhibit such large variations in their SAC responses.

Graphical Abstract

Correspondence: David Morgan, UCSF Genentech Hall Room N312B, 600 16th Street, San Francisco CA 94143, Tel: 415-476-6695, david.morgan@ucsf.edu.

[2]Current address: Hubrecht Institute, Royal Netherlands Academy of Arts and Sciences and University Medical Center Utrecht, Uppsalalaan 8, 3584 CT Utrecht, the Netherlands

*Co-corresponding authors

Supplemental Information

Supplemental Information includes one figure, Supplemental Experimental Procedures, and Supplemental References.

Author Contributions

M.G. designed and executed the experiments and wrote the paper, with guidance from D.O.M.

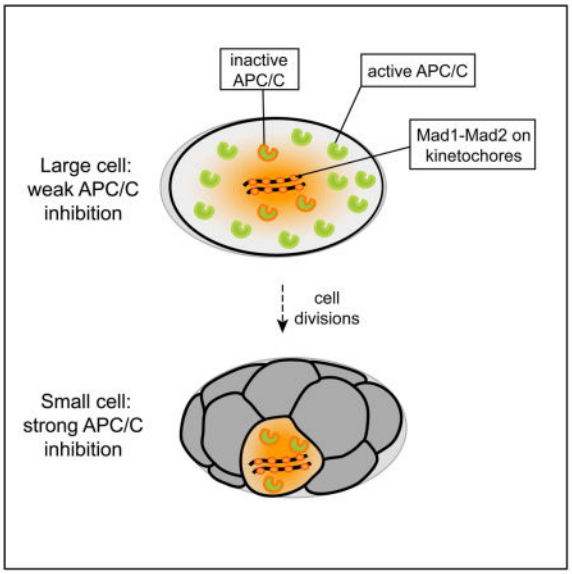

Introduction

Cell division requires an ordered series of events that culminates in the segregation of replicated chromosomes into two daughter cells. During early mitosis, sister chromatid pairs are held together by cohesin and aligned on the metaphase plate by attachment of their kinetochores to microtubules of the mitotic spindle. Upon correct attachment and bi-orientation of all kinetochores, cohesin is cleaved by the protease separase, and sister chromatids are pulled to opposite poles of the cell (Morgan, 2007; Nasmyth and Haering, 2009). This transition from metaphase to anaphase is triggered by the anaphase-promoting complex/cyclosome (APC/C), a ubiquitin-protein ligase that promotes the proteasomal destruction of mitotic substrates, including securin, an inhibitor of separase, and the mitotic cyclin, cyclin B. Destruction of securin and cyclin B leads to activation of separase and cleavage of cohesin, as well as dephosphorylation of Cdk substrates and mitotic exit (Morgan, 2007; Primorac and Musacchio, 2013; Sullivan and Morgan, 2007).

The key to successful anaphase is the timely activation of the APC/C, such that securin and cyclin B are degraded only after all sister chromatids have formed bipolar attachments to the spindle. This is achieved by a regulatory system called the spindle-assembly checkpoint (SAC), which delays APC/C activation when kinetochores are not properly attached to microtubules of the mitotic spindle (London and Biggins, 2014; Musacchio and Salmon, 2007; Primorac and Musacchio, 2013). During SAC signaling, unattached kinetochores recruit a complex of the checkpoint proteins Mad1 and Mad2, which generates a catalytic platform for the production of a mitotic checkpoint complex (MCC) consisting of Mad2, Cdc20, Bub3 and BubR1. The MCC directly inhibits the APC/C, thereby delaying anaphase onset (Chao et al., 2012; Izawa and Pines, 2015; London and Biggins, 2014).

In cells treated with microtubule poisons such as nocodazole, activation of the SAC causes a long-term arrest in mitosis. Ultimately, however, residual APC/C activity allows many cells

to “slip” out of mitosis despite continued SAC signaling – a process called mitotic checkpoint slippage (Gascoigne and Taylor, 2009; Rieder and Maiato, 2004). There is an enormous variation in the rate of mitotic slippage in different cell types. This large variation is well illustrated by the difference in SAC responses in newly fertilized embryonic cells of different metazoans: some embryos, such as those of *Xenopus laevis* or *Danio rerio*, display no SAC response during early embryonic divisions (Hara et al., 1980; Zhang et al., 2015); other embryonic cells, such as those of newly fertilized *C. elegans* or *Lytechinus variegatus* (green sea urchin) embryos, exhibit only moderate mitotic delays (Encalada et al., 2005; Sluder, 1979); and others, such as those of *Mus musculus*, *Arbacia punctulata* (purple-spined sea urchin) and *Spisula solidissima* (atlantic surf clam), seem to display strong checkpoint responses from the start of embryogenesis (Evans et al., 1983; Hunt et al., 1992; Siracusa et al., 1980; Wei et al., 2011). The absence of SAC signaling in some early embryonic divisions has been attributed to a developmental timer that only switches on SAC signaling at later stages of development, around the onset of gastrulation (Clute and Masui, 1995, 1997; Zhang et al., 2015). Another popular hypothesis is that the large size of many newly fertilized embryos results in dilution of the kinetochore-generated SAC signal, and that cells might need to reach a threshold kinetochore-to-cytoplasm ratio to generate a strong SAC signal (Minshull et al., 1994). However, there is currently no clear evidence *in vivo* to support this hypothesis.

Here, we explore how the strength of the SAC is determined during early embryogenesis of *C. elegans*. Our results show that there is a gradual increase in the strength of the SAC after each round of division, and we find that increasing kinetochore-to-cytoplasm ratio, rather than a developmental timer, is responsible for the strengthening SAC. These findings provide new insights into the large variations in mitotic progression that occur in different cells upon disruption of the mitotic spindle.

Results

The SAC becomes stronger after each embryonic division cycle

Previous studies have shown that disruption of the mitotic spindle during early embryonic divisions of *C. elegans* only slightly delays mitotic progression. Specifically, microtubule disruption at the two-cell stage delays the progression from nuclear envelope breakdown (NEB) to nuclear envelope reformation (NER) by 2.5-fold (Encalada et al., 2005). This moderate mitotic delay is dependent on signaling by the SAC, as depletion of checkpoint proteins Mad1 (MDF-1), Mad2 (MDF-2) or Mad3 (SAN-1) abolishes the delay (Encalada et al., 2005; Essex et al., 2009). To determine if all embryonic cell divisions in *C. elegans* exhibit this weak SAC response or if the strength of the SAC increases during later developmental stages, we measured the SAC response throughout early embryogenesis. Embryos expressing GFP-tubulin and mCherry-histone H2B were permeabilized by RNAi depletion of the permeability barrier component *perm-1* and treated with either 50 μM nocodazole or DMSO as a control (Figure 1). By direct addition of nocodazole during image acquisition, we could record the first failed division after treatment. Using GFP-tubulin exclusion from nuclei to determine the status of the nuclear envelope, we measured the time from NEB to NER in control and microtubule-depleted embryos (Figure 1A,B). Consistent

with previous results, we found that the time spent in mitosis for control embryos remained constant throughout the embryonic cycles (Figure 1A,C) (Arata et al., 2014). Strikingly, however, microtubule disruption resulted in an increasing arrest time in later embryonic divisions (Figure 1B,C).

To confirm that the mitotic delay depended on SAC signaling, we knocked out Mad3$^{san\text{-}1}$ by CRISPR/Cas9-mediated homologous recombination in our strain expressing GFP-tubulin and mCherry-histone H2B. Imaging of 16- and 32-cell embryos revealed that *san-1(mat5)* mutants were unable to arrest in mitosis after treatment with 50 μM nocodazole (Figure 1D). Thus, similar to what has been described for the 2-cell stage embryo (Encalada et al., 2005), SAC signaling is required for the mitotic arrests of later stage embryos.

Previous studies have shown that cells that slip out of mitosis in the absence of a spindle either (1) exit mitosis as a viable 4N cell but do not begin another round of cell division, (2) exit mitosis as a 4N cell and then undergo apoptosis in interphase, or (3) exit mitosis as a 4N cell and enter another cell cycle (Rieder and Maiato, 2004). We determined the fate of nocodazole-treated embryonic cells by continuing to observe 2- and 4-cell stage embryos after they had failed one division. We found that most (16/21) cells re-entered mitosis after a prolonged interphase and underwent a second mitotic arrest, which was always longer than the first (Figure 1E,F).

SAC strength correlates with cell volume during development

The increasing strength of the SAC in later embryonic stages could be explained by a gradual increase in expression of mitotic checkpoint regulators during development. However, our analyses revealed that embryonic age *per se* was not always a determinant of the strength of the SAC response: cells from different stages of development sometimes showed similar arrest times. To further characterize how cell size and SAC strength correlated, we performed experiments in embryos that expressed the membrane marker GFP-PH, allowing us to measure cell volume in embryos subjected to microtubule disruption (Figure 2A). In this genetic background, we observed a slightly stronger checkpoint than that seen in cells lacking the GFP-PH marker, but the results displayed a similar trend. Importantly, our measurements revealed a strong correlation between arrest time and cell volume (Figure 2B,C). The changes in arrest time were subtle in large cells, but became much more pronounced in later divisions when cell volume declined below a threshold of about 2 x 10^3 μm^3 (Figure 2C).

We noticed that the germline precursor cells, P1, P2 and P3, always had stronger checkpoints than other cells at the same stage (Figure 2D,E). One explanation is that these cells are the smallest cells at each division stage; however, we noticed that P cells arrested for longer times than would be predicted by their volume. For example, P cells arrested for similar times as significantly smaller Ab cell descendants of a generation later (Figure 2E,F). Thus, our data suggest that in germline precursor cells, in addition to a cell size-dependent SAC response, there are additional factors rendering these cells more sensitive to microtubule poisons.

The kinetochore-to-cytoplasm ratio determines SAC strength

To further demonstrate that cell size, and not a developmental timer, determines the strength of the SAC, we depleted *ani-2*, an anillin homolog that is specifically expressed in the gonad, to induce a broad variation in embryo sizes. Because double depletion of *ani-2* and *perm-1* resulted in very sick embryos, we were unable to perform nocodazole experiments in this background. Instead, we induced a SAC arrest by co-depletion of *zyg-1*, the Plk4 homolog, which results in monopolar spindles at the 2-cell stage because of a failure in centriole duplication after the first cell division (Essex et al., 2009; O'Connell et al., 2001). Whereas RNAi knockdown of *zyg-1* alone resulted in 2-cell stage embryos with sizes ranging from 4.3 x 10^3 μm^3 to 6.4 x 10^3 μm^3, co-depletion of *ani-2* and *zyg-1* resulted in a broad range of volumes between 1.6 x 10^3 μm^3 and 6.6 x 10^3 μm^3, corresponding to volumes that are typically observed in embryos between the 2- and 16-cell stages (Figure 3A,B). Measurement of mitotic delays induced by SAC activation again revealed that smaller cells displayed a longer mitotic arrest (Figure 3B). Thus, artificial reduction of cell size is sufficient to increase arrest time, suggesting that the stronger SAC we observe in small cells does not depend on developmental timing.

The increase in SAC strength in smaller cells could be explained by an increase in the ratio of the amount of unattached kinetochores, where the checkpoint signal is generated, to the amount of cytoplasm. Because our results showed that changing cell size is sufficient to alter the checkpoint response, we wondered whether changing the amount of kinetochores would also have an effect. To test this, we measured the checkpoint response in triploid embryos, which have 50% more kinetochores than wild-type diploid embryos. To generate triploid embryos, we mated *rec-8(ok978)* mutants, which fail the first meiotic division, with wild-type males, resulting in a homogenous population of triploid embryos (Figure 3C) (Severson et al., 2009). These triploid embryos had similar cell volumes as diploid control embryos obtained from crosses with heterozygote *rec-8(ok978)/nT1* (Figure S1). Depletion of *zyg-1* in these embryos resulted in arrest times at the 2-cell stage that were significantly longer than those of control diploid cells (Figure 3D). Thus, increasing the amount of chromosomes is sufficient to generate a stronger SAC signal.

A possible explanation for the longer arrest times in triploid embryos could be that a SAC inhibitory factor binds DNA, and that this factor is titrated away in cells with relatively more DNA, leading to a stronger checkpoint. In this case, the DNA-to-cytoplasm ratio, and not the kinetochore-to-cytoplasm ratio, would determine checkpoint strength. To distinguish between these two possibilities, we tested whether the presence of extra DNA alone is sufficient to induce a stronger checkpoint, or whether kinetochores need to be assembled on the DNA. We took advantage of the previous finding that DNA injected into *C. elegans* gonads is taken up into oocytes and embryos, where it forms extrachromosomal arrays (Mello et al., 1991). Initially, this DNA is packaged into chromatin but does not form neocentromeres and kinetochores, and is thus randomly partitioned during the first cell divisions in the embryo (Yuen et al., 2011). After multiple division cycles, in roughly the 16- or 32-cell stage embryo, the DNA arrays assemble de novo centromeres and acquire segregation competency, allowing them to be transmitted across generations (Yuen et al., 2011). To test whether the DNA-to-cytoplasm ratio or the kinetochore-to-cytoplasm ratio

determines checkpoint strength, we compared SAC arrest times in 2-cell stage temperature-sensitive *zyg-1(or409)* mutant embryos, either shortly after injection of DNA, or 2 generations after injection, in stably transmitting extrachromosomal lines (Figure 3E and 3F; see Supplemental Experimental Procedures). Our results revealed that shortly after injection, extra DNA, as visualized by DIC microscopy, was not able to prolong arrest times in monopolar divisions of *zyg-1(or409)* mutants ("+ DNA" in Figure 3F). In contrast, we observed a significant increase in SAC strength in embryos with stably segregating extrachromosomal arrays ("+ centromeric DNA" in Figure 3F). These results suggest that extra centromeres and kinetochores are required to increase SAC strength and thus that the kinetochore-to-cytoplasm ratio, and not the DNA-to-cytoplasm ratio, determines checkpoint strength in the embryo.

Cell size dependency of SAC strength occurs downstream of kinetochore recruitment of Mad1

We hypothesized that the cell size dependency of the SAC could manifest either at the assembly of checkpoint proteins at the unattached kinetochore or downstream of kinetochore assembly (for example, at the level of MCC binding to the APC/C). To test for cell size dependence in the ability of unattached kinetochores to recruit checkpoint proteins, we quantified the kinetochore localization of the Mad1 homolog MDF-1. In *C. elegans*, SAC activation leads to the enrichment of $Mad1^{MDF-1}$ on unattached kinetochores, which span the entire length of holocentric chromosomes. We determined the amount of kinetochore-localized GFP-$Mad1^{MDF-1}$ relative to the chromosome marker mCherry-H2B in nocodazole-treated *perm-1* RNAi embryos. The amount of kinetochore $Mad1^{MDF-1}$ was similar in early-stage and late-stage embryos (Figure 4A,B). Thus, the cell size-dependent strengthening of the SAC does not result from increased $Mad1^{MDF-1}$ recruitment to the unattached kinetochore, suggesting that unattached kinetochores are equally competent in large or small cells to activate the SAC.

Our results thus far indicate that the kinetochore-to-cytoplasm ratio determines the strength of the SAC during embryogenesis. This suggests that the stronger SAC in small cells is achieved by inhibition of a larger fraction of APC/C in small cells. If this were the case, we might not expect the concentrations of checkpoint proteins and APC/C to differ between large or small cells. To test this hypothesis, we measured cytoplasmic fluorescence intensities of GFP-tagged $Mad1^{MDF-1}$, $Mad2^{MDF-2}$ and the APC/C subunit $Apc1^{MAT-3}$ in prometaphase/metaphase cells of early and late stage embryos. We found no significant differences in the cytoplasmic concentrations of these proteins during early (1 to 4 cell stage) or late (16 to 64 cell stage) embryonic stages (Figure 4C,D). Thus, cytoplasmic Mad1, Mad2 and Apc1 concentrations are constant during early embryonic divisions, indicating that their total amounts per cell decrease with each division. These results, together with our analysis of Mad1 at kinetochores, suggest that decreasing cell size leads to an increase in the ratio of kinetochore Mad1 to cytoplasmic APC/C.

Discussion

Recent kinetic analyses of SAC signaling in cells treated with a variety of microtubule poisons have demonstrated that the SAC response is not all-or-nothing but rather varies in strength depending on the amount of unattached kinetochores (Collin et al., 2013; Dick and Gerlich, 2013). Increased disruption of the mitotic spindle creates more unattached kinetochores, resulting in increased recruitment of checkpoint proteins and therefore stronger APC/C inhibition and a longer time before cells are able to exit mitosis (Collin et al., 2013). The observation of a graded SAC response raises the possibility that other parameters may tune the extent of APC/C inhibition by checkpoint proteins. Indeed, our analysis demonstrates that cell size modulates SAC signaling: decreasing cell size leads to stronger checkpoint responses, even when all kinetochores are unattached. Whereas the number of unattached kinetochores affects SAC strength by determining how many checkpoint proteins are recruited to kinetochores, the cell size-dependent response described here is likely to operate downstream of recruitment, as we observe that the amount of Mad1 protein recruited to unattached kinetochores is equal in cells of different sizes.

A potential explanation for the weaker checkpoint in larger cells is that the kinetochore-generated checkpoint signal, which consists of Mad2 in a complex with Cdc20 and other proteins, is constantly being disassembled in the cytoplasm. If we assume that the soluble concentration of the disassembly activity remains constant in all cells, then one might predict a weaker checkpoint in cells where the relative amount of checkpoint-generating platform (the kinetochore) is limiting, and a stronger checkpoint in cells with a higher ratio of kinetochore to cytoplasm. A similar dependency on the kinetochore-to-cytoplasm ratio would result if soluble disassembly activities or other checkpoint inhibitors are inactivated by association with kinetochores.

It is unlikely that the kinetochore-to-cytoplasm ratio is the only determinant of SAC strength during development. Recent studies of mitotic progenitor cell divisions in the *C. elegans* germline have revealed that these cells have strong SAC responses, which are highly sensitive to organismal physiological changes such as dietary intake (Gerhold et al., 2015). We also found evidence for cell-type specific SAC responses, as we find that the germ cell precursors (P cells) have a slightly stronger checkpoint than would be expected just from their size alone. However, these cells still respond to changes in size, and our analysis suggests that the kinetochore-to-cytoplasm ratio is generally the strongest predictor of the SAC response during early embryogenesis of *C. elegans*.

In species where there is no SAC response during early embryogenesis, it has been shown that SAC competence is acquired in the developmental stages just prior to gastrulation, when cell cycles start to lengthen. Although this developmental time could correspond to the stage when the nuclear-to-cytoplasm ratio reaches a particular threshold required for efficient SAC signaling, studies that have uncoupled the nuclear-to-cytoplasm ratio from developmental timing suggest that a developmental clock is the predominant mechanism controlling SAC strength in *X. laevis* and *D. rerio* (Clute and Masui, 1995, 1997; Zhang et al., 2015). Nonetheless, checkpoint proteins XMad1 and XMad2 are present in *X. laevis* early embryos, and a strong SAC arrest can be induced artificially by addition of nocodazole

and sperm nuclei at a density similar to the nuclear-to-cytoplasm ratio of somatic cells (Chen et al., 1998; Chen et al., 1996; Minshull et al., 1994). This artificial SAC response depends on the presence of embryonic XMad1 and XMad2 (Chen et al., 1998; Chen et al., 1996), suggesting that although SAC signaling is not apparent in early embryonic cycles of some organisms, it may be masked by a low kinetochore-to-cytoplasm ratio. Our analysis in *C. elegans* indicates that the strengthening of the SAC with decreasing size is not linear across the whole range of cell volumes; we observe only modest mitotic delays in the one- and two-cell stage embryos. The fact that *C. elegans* has holocentric chromosomes, and thus a higher amount of kinetochores per cell, and that its embryos are more than 20 times smaller than *X. laevis* embryos, could explain why *C. elegans* has a detectable SAC response from the first embryonic division, whereas *X. laevis* does not. Understanding whether the kinetochore-to-cytoplasm ratio has any function in controlling the strength of the SAC in embryos other than those of *C. elegans* will require a detailed systematic analysis of mitotic timing in the presence of microtubule drugs during different stages of development.

Experimental procedures

Microscopy

Strain construction, RNAi methods, and DNA injection methods are described in Supplemental Experimental Procedures. For nocodazole treatment of embryos, *C. elegans* young adults were placed on *perm-1* RNAi plates for 16–20 h at 15°C and then dissected onto a coverslip containing 0.7–0.8x diluted egg salts buffer (118 mM NaCl, 48 mM KCl) supplemented with 10 mM PIPES pH 7.3, 1 mM ATP and 10 mM sucrose. Embryos and adult carcasses were carefully pipetted into two wells of a 96-well plate with glass bottom (Matriplate MGB096) that had been coated with 0.1% Poly-L-Lysine solution (Sigma P8920) and extensively washed thereafter. Embryos were imaged either in the UCSF Nikon Imaging Center using a Plan Apo VC 60x/1.4 Oil objective on an inverted Nikon Ti-E microscope equipped with a Yokagawa CSU22 spinning disk, the Nikon Perfect Focus system, a Photometrics Evolve Delta EMCCD camera, and microManager software (Edelstein et al., 2010) or in the Hubrecht Imaging Center on a PerkinElmer Ultraview VoX spinning disk microscope using Volocity software. Multiple positions from each well were imaged every 1 to 3 min, and for each position a 20 μm Z-stack was taken with 2 μm steps (or 1 μm steps for $Mad1^{MDF-1}$-GFP imaging). After initiation of imaging, usually before the 5^{th} time point, DMSO or nocodazole was added to individual wells from a 5x stock to a final concentration of 50 μM (or 2.5% final DMSO concentration). All imaging was performed at 25°C, and usually lasted 1–2 h. Images were only used for analysis when control DMSO treated embryos continued to divide over the entire imaging session.

For experiments in which *zyg-1* RNAi or the zyg-*1(or409)* allele was used to induce a 2-cell stage SAC response, animals were dissected on a coverslip with egg salts buffer and either transferred to a well of a Poly-L-lysine 96-well plate as described above, or onto a 2% agarose pad. These embryos were imaged using either a Plan Apo VC 100x / 1.4 Oil objective on a Nikon Ti microscope equipped with the Nikon Perfect Focus system, a ScopeLED BrightField Microscope Illuminator, and an Andor Zyla camera, or on a Leica DM6000 upright microscope with a HCX Plan Apo 63x / 1.3 Glycerol objective and a Leica

DFC360FX camera. Multiple embryos were imaged from the one-cell or early two-cell stage onwards using differential interference contrast (DIC) microscopy. A 20 μm Z-stack was taken with 0.5 μm steps every minute for multiple positions, using 10 ms brightfield exposure at the lowest setting of the LED illuminator.

Image analysis

Analysis of mitotic timings in embryos treated with nocodazole or *zyg-1* RNAi was manually performed on raw data using micromanager software. Cells were tracked as they proceeded from nuclear envelope breakdown (NEB, visualized by the redistribution of GFP-tubulin signal into the former nucleus, or by direct visualization of nuclear envelope disassembly by DIC) to nuclear envelope reformation (NER, visualized by the exclusion of GFP from the nucleus or reassembly of the nuclear envelope by DIC). For quantification of cell sizes, we measured the areas of cross sections at the top (A1), middle (M) and bottom (A2) of each cell, and cell volumes were calculated as prismatoids, using 1/6h(A1+4M+A2), where h was the height of each cell, determined by how many Z planes it spanned (Decker et al., 2011).

ImageJ software was used for quantification of Mad1^{MDF-1}-GFP intensities on kinetochores. A subset of embryos (2 out of 7 embryos) was excluded from the analysis, as these embryos displayed very short arrest times in nocodazole and thus did not reflect wild-type behavior. Indeed, the OD1209 strain carrying Mad1^{MDF-1}-GFP has been reported to have a somewhat compromised checkpoint response (Moyle et al., 2014), so we only quantified embryos that displayed arrest times within the normal range for their particular stage. From these embryos, we used images of cells that were taken 5 min after NEB, and Z-stack projections were made of the planes where we observed mCherry-H2B signal (generally 3 or 4 planes, 1 μm apart). From the Z-projections, chromosomal areas were selected and average intensities of GFP and mCherry signals were measured. Background intensities of the green and red channel in a 10 μm x 10 μm area outside the embryo were processed in the same manner, and subtracted from Mad1^{MDF-1}-GFP and mCherry-H2B intensities. From these values, the ratio of Mad1^{MDF-1}-GFP to mCherry-H2B was calculated.

For quantification of cytoplasmic GFP-Mad1^{MDF-1}, GFP-Mad2^{MDF-2} and Apc1^{MAT-2}-GFP intensities, Z-projections of 3 planes, 1 μm apart, were made of prometaphase and metaphase cells. Fluorescence intensities of GFP signals in 3 cytoplasmic areas, outside the mitotic spindle, were measured and averaged. Background intensities were subtracted from cytoplasmic intensities.

Supplementary Material

Refer to Web version on PubMed Central for supplementary material.

Acknowledgments

We are grateful to Kaveh Ashrafi and his lab members for the use of their laboratory equipment, reagents and support. We thank the labs of Karen Oegema and Arshad Desai for helpful discussions and the GFP-Mad1^{MDF-1} and GFP-Mad2^{MDF-2} strains, Laura Rosen for critical reading of the manuscript, members of the Morgan lab for fruitful discussions, and Kurt Thorn and DeLaine Larsen of the UCSF Nikon Imaging Center for their help with microscopy. Some strains were provided by the *Caenorhabditis* Genetics Center (CGC), which is funded by NIH

Office of Research Infrastructure Programs (P40 OD010440). Imaging was performed at the Nikon Imaging Center at UCSF and the Hubrecht Imaging Center. This work was supported by funding to M.G. from the Human Frontiers Science Program (HFSP) and the Dutch Cancer Society (KWF), and funding to D.O.M. from the National Institute of General Medical Sciences (R01-GM094173).

References

Arata Y, Takagi H, Sako Y, Sawa H. Power law relationship between cell cycle duration and cell volume in the early embryonic development of Caenorhabditis elegans. Front Physiol. 2014; 5:529. [PubMed: 25674063]

Chao WC, Kulkarni K, Zhang Z, Kong EH, Barford D. Structure of the mitotic checkpoint complex. Nature. 2012; 484:208–213. [PubMed: 22437499]

Chen RH, Shevchenko A, Mann M, Murray AW. Spindle checkpoint protein Xmad1 recruits Xmad2 to unattached kinetochores. J Cell Biol. 1998; 143:283–295. [PubMed: 9786942]

Chen RH, Waters JC, Salmon ED, Murray AW. Association of spindle assembly checkpoint component XMAD2 with unattached kinetochores. Science. 1996; 274:242–246. [PubMed: 8824188]

Clute P, Masui Y. Regulation of the appearance of division asynchrony and microtubule-dependent chromosome cycles in Xenopus laevis embryos. Dev Biol. 1995; 171:273–285. [PubMed: 7556912]

Clute P, Masui Y. Microtubule dependence of chromosome cycles in Xenopus laevis blastomeres under the influence of a DNA synthesis inhibitor, aphidicolin. Dev Biol. 1997; 185:1–13. [PubMed: 9169045]

Collin P, Nashchekina O, Walker R, Pines J. The spindle assembly checkpoint works like a rheostat rather than a toggle switch. Nat Cell Biol. 2013; 15:1378–1385. [PubMed: 24096242]

Decker M, Jaensch S, Pozniakovsky A, Zinke A, O'Connell KF, Zachariae W, Myers E, Hyman AA. Limiting amounts of centrosome material set centrosome size in C. elegans embryos. Curr Biol. 2011; 21:1259–1267. [PubMed: 21802300]

Dick AE, Gerlich DW. Kinetic framework of spindle assembly checkpoint signalling. Nat Cell Biol. 2013; 15:1370–1377. [PubMed: 24096243]

Edelstein A, Amodaj N, Hoover K, Vale R, Stuurman N. Computer control of microscopes using microManager. Curr Protoc Mol Biol. 2010; Chapter 14(Unit14):20. [PubMed: 20890901]

Encalada SE, Willis J, Lyczak R, Bowerman B. A spindle checkpoint functions during mitosis in the early Caenorhabditis elegans embryo. Mol Biol Cell. 2005; 16:1056–1070. [PubMed: 15616189]

Essex A, Dammermann A, Lewellyn L, Oegema K, Desai A. Systematic analysis in Caenorhabditis elegans reveals that the spindle checkpoint is composed of two largely independent branches. Mol Biol Cell. 2009; 20:1252–1267. [PubMed: 19109417]

Evans T, Rosenthal ET, Youngblom J, Distel D, Hunt T. Cyclin: a protein specified by maternal mRNA in sea urchin eggs that is destroyed at each cleavage division. Cell. 1983; 33:389–396. [PubMed: 6134587]

Gascoigne KE, Taylor SS. How do anti-mitotic drugs kill cancer cells? J Cell Sci. 2009; 122:2579–2585. [PubMed: 19625502]

Gerhold AR, Ryan J, Vallee-Trudeau JN, Dorn JF, Labbe JC, Maddox PS. Investigating the regulation of stem and progenitor cell mitotic progression by in situ imaging. Curr Biol. 2015; 25:1123–1134. [PubMed: 25819563]

Hara K, Tydeman P, Kirschner M. A cytoplasmic clock with the same period as the division cycle in Xenopus eggs. Proc Natl Acad Sci U S A. 1980; 77:462–466. [PubMed: 6928638]

Hunt T, Luca FC, Ruderman JV. The requirements for protein synthesis and degradation, and the control of destruction of cyclins A and B in the meiotic and mitotic cell cycles of the clam embryo. J Cell Biol. 1992; 116:707–724. [PubMed: 1530948]

Izawa D, Pines J. The mitotic checkpoint complex binds a second CDC20 to inhibit active APC/C. Nature. 2015; 517:631–634. [PubMed: 25383541]

London N, Biggins S. Signalling dynamics in the spindle checkpoint response. Nat Rev Mol Cell Biol. 2014; 15:736–747. [PubMed: 25303117]

Mello CC, Kramer JM, Stinchcomb D, Ambros V. Efficient gene transfer in C.elegans: extrachromosomal maintenance and integration of transforming sequences. EMBO J. 1991; 10:3959–3970. [PubMed: 1935914]

Minshull J, Sun H, Tonks NK, Murray AW. A MAP kinase-dependent spindle assembly checkpoint in Xenopus egg extracts. Cell. 1994; 79:475–486. [PubMed: 7954813]

Morgan, DO. The cell cycle : principles of control. London Sunderland, MA: New Science Press ; Sinauer Associates; 2007.

Moyle MW, Kim T, Hattersley N, Espeut J, Cheerambathur DK, Oegema K, Desai A. A Bub1-Mad1 interaction targets the Mad1-Mad2 complex to unattached kinetochores to initiate the spindle checkpoint. J Cell Biol. 2014; 204:647–657. [PubMed: 24567362]

Musacchio A, Salmon ED. The spindle-assembly checkpoint in space and time. Nat Rev Mol Cell Biol. 2007; 8:379–393. [PubMed: 17426725]

Nasmyth K, Haering CH. Cohesin: its roles and mechanisms. Annu Rev Genet. 2009; 43:525–558. [PubMed: 19886810]

O'Connell KF, Caron C, Kopish KR, Hurd DD, Kemphues KJ, Li Y, White JG. The C. elegans zyg-1 gene encodes a regulator of centrosome duplication with distinct maternal and paternal roles in the embryo. Cell. 2001; 105:547–558. [PubMed: 11371350]

Primorac I, Musacchio A. Panta rhei: the APC/C at steady state. J Cell Biol. 2013; 201:177–189. [PubMed: 23589490]

Rieder CL, Maiato H. Stuck in division or passing through: what happens when cells cannot satisfy the spindle assembly checkpoint. Dev Cell. 2004; 7:637–651. [PubMed: 15525526]

Severson AF, Ling L, van Zuylen V, Meyer BJ. The axial element protein HTP-3 promotes cohesin loading and meiotic axis assembly in C. elegans to implement the meiotic program of chromosome segregation. Genes Dev. 2009; 23:1763–1778. [PubMed: 19574299]

Siracusa G, Whittingham DG, De Felici M. The effect of microtubule- and microfilament-disrupting drugs on preimplantation mouse embryos. J Embryol Exp Morphol. 1980; 60:71–82. [PubMed: 7198136]

Sluder G. Role of spindle microtubules in the control of cell cycle timing. J Cell Biol. 1979; 80:674–691. [PubMed: 572367]

Sullivan M, Morgan DO. Finishing mitosis, one step at a time. Nat Rev Mol Cell Biol. 2007; 8:894–903. [PubMed: 17912263]

Wei Y, Multi S, Yang CR, Ma J, Zhang QH, Wang ZB, Li M, Wei L, Ge ZJ, Zhang CH, et al. Spindle assembly checkpoint regulates mitotic cell cycle progression during preimplantation embryo development. PLoS One. 2011; 6:e21557. [PubMed: 21720555]

Yuen KW, Nabeshima K, Oegema K, Desai A. Rapid de novo centromere formation occurs independently of heterochromatin protein 1 in C. elegans embryos. Curr Biol. 2011; 21:1800–1807. [PubMed: 22018540]

Zhang M, Kothari P, Lampson MA. Spindle assembly checkpoint acquisition at the mid-blastula transition. PLoS One. 2015; 10:e0119285. [PubMed: 25741707]

Highlights

- In *C. elegans* embryos, small cells have a stronger spindle assembly checkpoint
- Checkpoint strength increases in mutants with small cell size or increased ploidy
- The amount of checkpoint-generating kinetochore signal is unaffected by cell size
- Checkpoint strength is determined by the ratio of kinetochore signal to cytoplasm

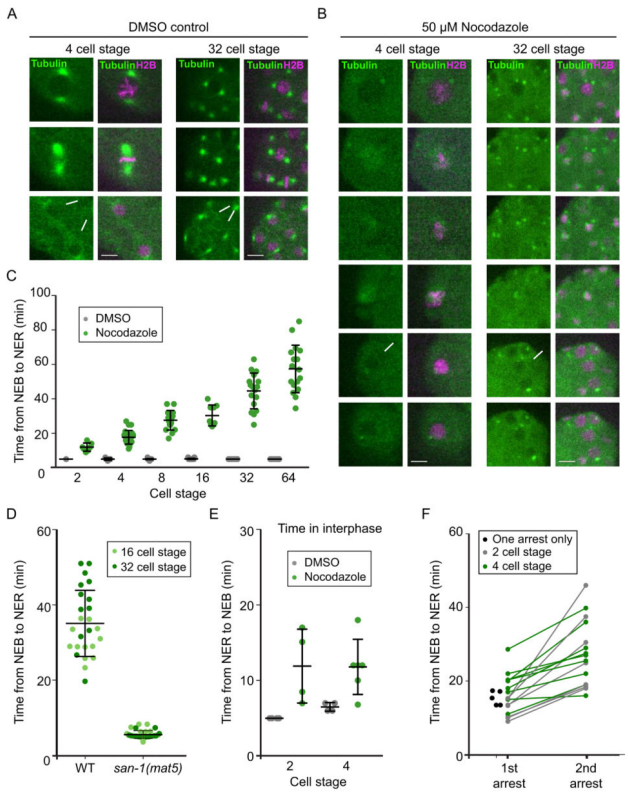

Figure 1. The SAC response becomes stronger after each embryonic division in *C. elegans*

(A–B) Still images from time-lapse video of control (A) or nocodazole-treated (B) embryonic cells expressing GFP-Tubulin (green) and mCherry-H2B (magenta) as they enter and exit mitosis. Asterisks mark the redistribution of GFP-Tubulin at NEB, and arrows point to the exclusion of GFP-tubulin at NER. For late cell stages (right panels), arrowheads in the merged images mark the cell that is being followed from NEB to NER. Time is in min:s, where 0:00 is the frame when NEB is first visible. Scale bars represent 5 µm.

(C) Quantification of mitotic timings from control (grey dots) and nocodazole-treated embryos (green dots). Individual measurements are shown with mean (middle bar) and standard deviation (error bars).

(D) Quantification of mitotic timings from control (wild type) and Mad3$^{san\text{-}1}$ deletion mutants (*san-1(mat5)*). Only cells from 16- (light green) or 32-cell stage embryos (dark green) were quantified. Individual measurements are shown with mean (middle bar) and standard deviation (error bars).

(E) Quantification of times spent in interphase (from NER to NEB of next division) of DMSO-treated controls and nocodazole-treated embryos. Only Ab cells and their descendants were quantified. Individual measurements are shown with mean (middle bar) and standard deviation (error bars).

(F) Quantification of mitotic timings of cells from 2- and 4-cell stage embryos that were followed after nocodazole treatment and mitotic exit. Arrest times are shown for the first and second mitotic arrest, individual cells are connected by lines. Cells that did not re-enter a second mitosis are depicted as black dots.

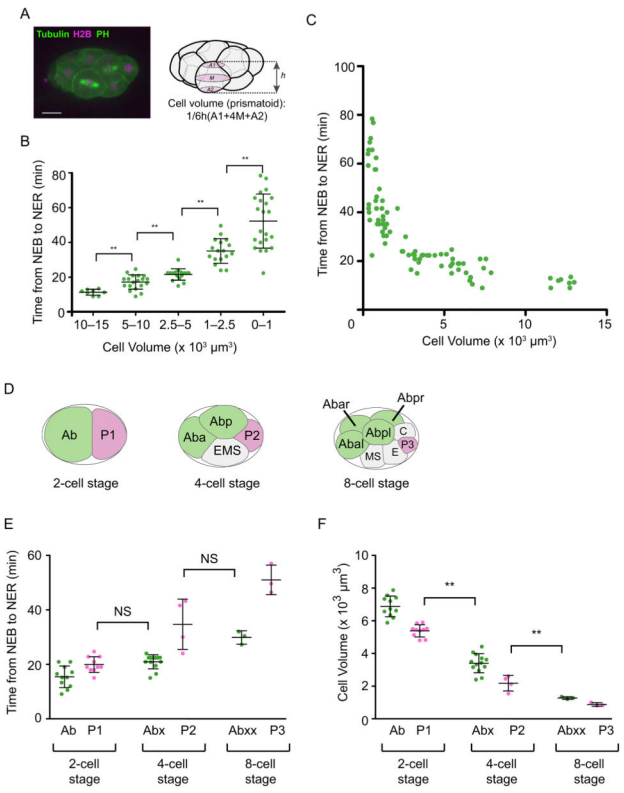

Figure 2. The SAC response correlates with cell volume

(A) Still image of an embryo expressing GFP-tubulin, mCherry-H2B and GFP-PH (left) and schematic illustration of volume calculations (right; see Experimental Procedures).

(B–C) Quantification of SAC arrest times in nocodazole-treated embryos as a function of cell volume. Each dot represents time from NEB to NER in a single cell, and its corresponding volume range (B) or exact volume measurement (C). In (B), individual measurements are shown with mean (middle bar) and standard deviation (error bars) (**p < 0.01, Student's *t*-test).

(D) Schematic of 2-, 4- and 8-cell stage embryos with cell names. Ab cell and Ab cell descendants are colored green, P cells are colored pink.

(E) Individual arrest times are shown for Ab cells, Ab descendants (green) and P cells (pink) at the 2-, 4- and 8-cell stage. Individual measurements are shown with mean (middle bar) and standard deviation (error bars). (NS, not significant, p > 0.05, Student's *t*-test).

(F) Cell volumes are shown for Ab cells, Ab descendants (green) and P cells (pink) at the 2-, 4- and 8-cell stage. Individual measurements are shown with mean (middle bar) and standard deviation (error bars) (**p < 0.01, Student's *t*-test).

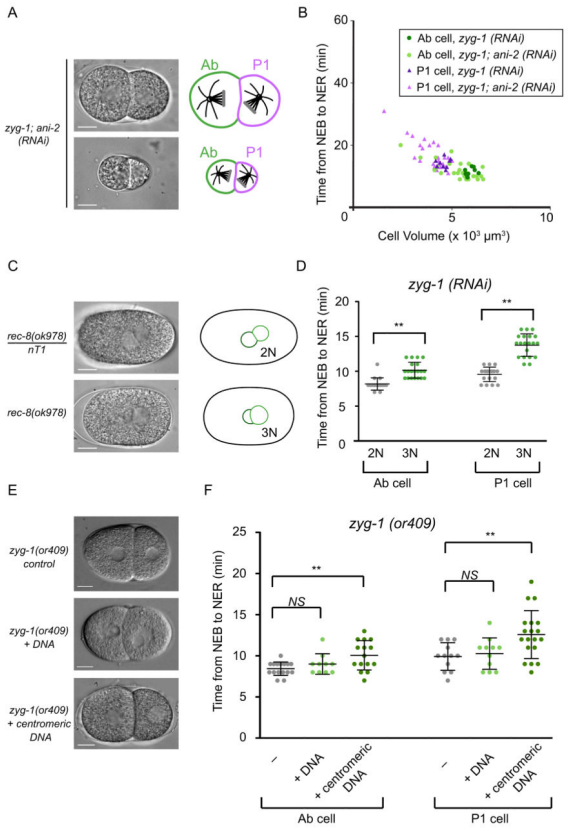

Figure 3. SAC strength is determined by cell size and amount of kinetochores

(A) Two examples of differently sized *ani-2; zyg-1* (RNAi) embryos at the 2-cell stage (left) and schematic of monopolar division (right). Scale bars represent 10 µm.

(B) Quantification of arrest times of 2-cell stage *zyg-1* (RNAi) and *ani-2; zyg-1* (RNAi) embryos undergoing monopolar divisions. Each dot/triangle represents a single cell; dots are Ab cells and triangles are P1 cells.

(C) Still images (left) and schematics (right) of a control diploid embryo from a heterozygote *rec-8(ok978)/nT1* parent (top) and a triploid embryo from a homozygote *rec-8(ok978)* parent (bottom). In *rec-8(ok978)* homozygote mutant embryos, maternal and paternal pronuclei are different sizes due to failed polar body extrusion in female meiosis II, resulting in the contribution of one extra set of chromosomes by the female. Scale bars represent 10 µm.

(D) Quantification of Ab and P1 arrest times of diploid and triploid embryos depleted of *zyg-1* by RNAi. Individual measurements are shown with mean (middle bar) and standard deviation (error bars) (**p < 0.01, Student's *t*-test). Cell size was the same in diploid and triploid cells (Fig. S1).

(E) Still images of *zyg-1 (or409)* temperature-sensitive embryos shifted to the non-permissive temperature 30 minutes prior to imaging. The top embryo is a non-injected control, the middle embryo is from an adult that had been injected with DNA 5 hours before imaging, and the bottom embryo is from an adult stably transmitting extrachromosomal DNA. For the "+ DNA" embryos, only those embryos in which extra DNA was visible by

DIC microscopy (white arrowheads) were included in the quantification (see F). Scale bars represent 10 μm.

(F) Quantification of Ab and P1 arrest times of control *zyg-1 (or409)* embryos (non-injected, "−"), *zyg-1 (or409)* embryos injected with DNA and imaged shortly after injection ("+ DNA"), and *zyg-1 (or409)* embryos that stably segregated extrachromosomal arrays ("+ centromeric DNA"). For the latter group, embryos from 3 independent lines were scored. Individual measurements are shown with mean (middle bar) and standard deviation (error bars) (NS, not significant, $p > 0.05$, and **, $p < 0.01$, Student's *t*-test).

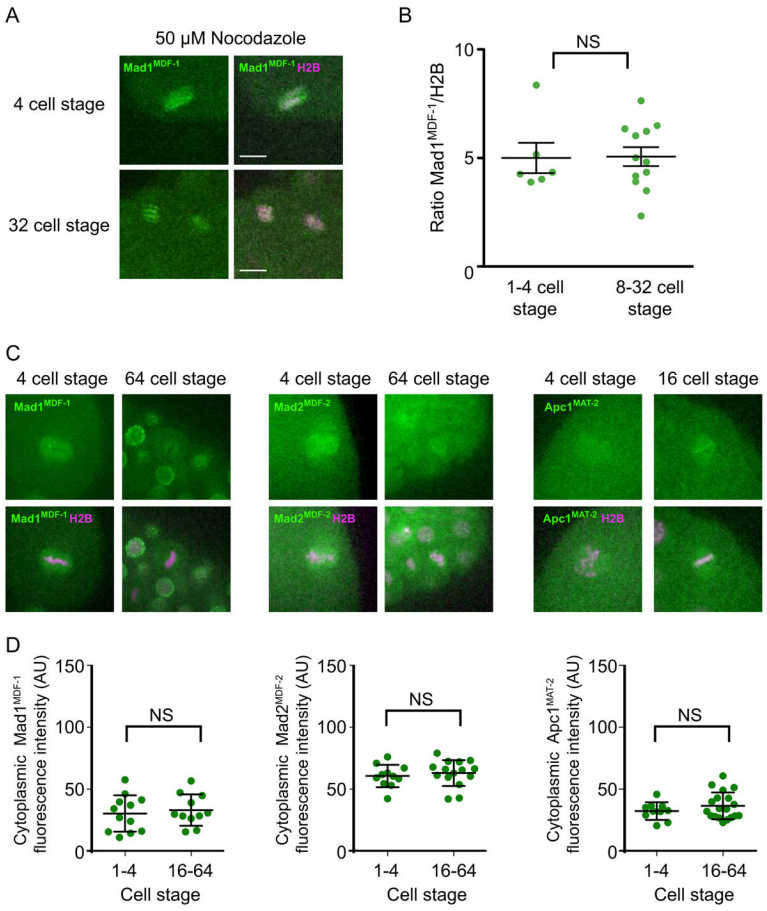

Figure 4. Mad1^{MDF-1} localization to unattached kinetochores does not depend on cell size

(A) Representative images of nocodazole-treated early stage (top) and late stage (bottom) embryos expressing GFP-Mad1^{MDF-1} (green) and mCherry-H2B (magenta). Scale bars represent 5 μm.

(B) Ratio of relative fluorescence intensities of GFP-Mad1^{MDF-1} / mCherry-H2B on chromosomes of early (1–4 cell) and late (8–32 cell) stage embryos treated with 50 μM nocodazole. Individual measurements are shown with mean (middle bar) and standard deviation (error bars) (NS, not significant, $p > 0.05$, Student's *t*-test).

(C) Representative images of prometaphase or metaphase cells of early and late stage embryos expressing GFP-Mad1^{MDF-1} (left panel), GFP-Mad2^{MDF-2} (middle panel) and Apc1^{MAT-2}-GFP (right panel). mCherry-H2B is shown in magenta. For late cell stages (right panels), arrowheads mark cells in prometaphase. Scale bar represents 5 μm.

(D) Quantification of fluorescent intensities of cytoplasmic GFP-Mad1^{MDF-1} (left panel), GFP-Mad2^{MDF-2} (middle panel) and Apc1^{MAT-2}-GFP (right panel). Regions of cytoplasm outside the mitotic spindle were analyzed, and so these measurements do not include GFP-tagged proteins on the spindle. Individual measurements are shown with mean (middle bar) and standard deviation (error bars) (NS, not significant, $p > 0.05$, Student's *t*-test). AU, arbitrary unit.